Preprints of the 21st IFAC World Congress (Virtual)
Berlin, Germany, July 12-17, 2020

Flatness-based MPC for underactuated surface vessels in confined areas

Simon Helling Max Lutz Thomas Meurer

Chair of Automatic Control, Kiel University, Kaiserstr. 2, 24103 Kiel, Germany (e-mail: {sh, mlut, tm}@tf.uni-kiel.de).

Abstract: A two-phase model predictive controller (MPC) is proposed for underactuated surface vessel operation in confined environments. For general driving maneuvers (phase one) the ship's geometry is not considered explicitly while in more restricted areas (stage two) which occur, e.g., in mooring maneuvers, the ship's geometry is approximated to ensure collision avoidance. To remove the dynamical constraint in the problem setup, the differential flatness of the fully actuated system is exploited and the flat outputs are parameterized using B-spline functions. Underactuated behavior is retained by means of inequality constraints that are imposed on the non-controllable input. In an effort to solve the MPC, a static nonlinear optimization problem is formulated and feasibility w.r.t. obstacles and actuator constraints is ensured at collocation points. Static obstacles are considered as constructive solid geometry functions in the MPC which also takes into account disturbances induced by wind.

Keywords: Surface vessel, optimal control, flatness, model predictive control, constrained environment, ship motion control, autonomous vehicle, docking.

1. INTRODUCTION

Recent years show an advancing interest in the field of autonomous vessels. This is due to the variety of challenging applications where autonomous systems can be advantageous to humanly-operated vessels but also because of the task to solve the arising complex problems that involve environmental disturbances and nonlinear vessel dynamics, see Streng and Kuipers (2020).

Along with classical path-following scenarios using PID controllers as shown in Bårslett et al. (2018), more advanced approaches such as Lyapunov-based methods involving, e.g., passivity and backstepping techniques were applied in Fossen et al. (2002); Breivik and Fossen (2004); Do and Pan (2006, 2009); Fossen (2011). Furthermore, exact feedback linearization and differential flatness were exploited in Agrawal and Sira-Ramirez (2004); de Aquino Limaverde Filho and Fortaleza (2013); Paliotta et al. (2018). In general, the mentioned approaches are not able to handle input and state constraints. To deal with such issues, a third branch has emerged which utilizes optimization-based techniques, see, e.g., Bitar et al. (2018, 2019); Lekkas et al. (2016). Essentially, optimization-based methods aim to minimize a cost functional depending on the control inputs subject to the system dynamics and additional equality and inequality constraints. Methods to solve this optimal control problem (OCP) can be characterized as indirect or direct, where the former leads to a two-point boundary value problem and the latter directly minimizes the cost functional by suitable discretization.

While nonlinear and optimization-based techniques constitute independent methods, their combination can lead to increased performance and reduced complexity. This combined approach goes back to Agrawal and Faiz (1998) and was further extended to the class of differentially flat systems, e.g. in Milam et al. (2000). Herein, the so-called flat outputs are parameterized with B-spline functions to obtain an OCP, where the constraint imposed by the system dynamics is implicitly fulfilled. Therefore, this constraint can be omitted in the problem setup. Subsequent discretization in time transfers the OCP to a static optimization problem (direct method). This approach has already been used for fuel optimization in hybrid electric drives and trajectory generation for quadrocopters, see Abel and Joševski (2015) and Abel et al. (2016), respectively.

In this contribution, the combined flatness and optimization approach is extended and applied to an underactuated surface vessel model. In Agrawal and Sira-Ramirez (2004) the flatness of the considered model is verified under restrictive assumptions on the model parameters. Moreover, the resulting flat state and input parameterizations contain several singularities, which severely restrict its applicability. To address this in the following the so-called defect elimination method is used as suggested, e.g., in Oldenburg and Marquardt (2002). Utilizing this approach, the underactuated dynamics is achieved by means of the singularity free flat parameterization obtained for a fully actuated vessel model. This comes at the cost of an additional equality constraint that must be imposed on the parameterized, non-controllable input. For practical reasons, however, this equality constraint is replaced by two inequality constraints. This approach is evaluated for driving maneuvers in confined environments including mooring based on closed-loop MPC involving disturbances induced by wind. Herein, the maneuver is separated into two phases. The first phase will be referred to as the driving phase where the ship geometry is not explicitly

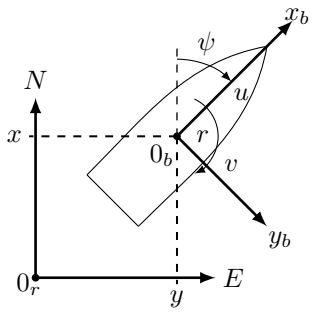

Fig. 1. Vessel position and orientation in NED frame and velocities in body-fixed frame for 3DOF surface vessel.

considered to evaluate obstacle collisions. Subsequently, the second phase will be referred to as the mooring phase, where the ship geometry is approximated to ensure obstacle avoidance for the entire ship hull.

The paper is organized as follows. The vessel model is introduced in Section 2 together with its flat state and input parameterization. Section 3 describes the general form of an OCP and introduces the used approach for obstacle modeling with constructive solid geometry (CSG) functions. Additionally, the flatness-based direct solution method is described by briefly introducing the main properties of B-spline functions and formulating their connection to flat outputs. To account for wind-induced disturbances, the extension to MPC is proposed in Section 4. Subsequently, a two-phase MPC is presented together with short remarks on the used disturbance model which is assumed to be unknown to the MPC. Finally, Section 5 shows simulation results and the paper closes with some conclusions in Section 6.

2. SURFACE VESSEL MODEL

Assuming that the vessel operates in calm sea conditions, e.g., in harbor areas or near shore shipping applications, roll, pitch and heave velocities can be neglected. This results in a three degrees of freedom (3DOF) description of a surface vessel for which two sets of coordinates are required. The first set $\boldsymbol{\eta} = [x\ y\ \psi]^{\mathrm{T}}$ describes the vessel location and pose in the North-East-Down (NED) frame with origin 0_r, where x corresponds to the north and y to the east coordinate. The third component ψ describes the vessel orientation w.r.t. the north axis. This set of coordinates is a reference frame for the second set of coordinates $\boldsymbol{\nu} = [u\ v\ r]^{\mathrm{T}}$ which represents the vessels surge and sway velocities as well as its yaw rate in a body-fixed coordinate frame, respectively. These relations can be observed in Fig. 1.

2.1 Vessel dynamics

By applying Newton's second law the equations of motion for a surface vessel can be described using matrix-vector notation, see Fossen et al. (2002), in the form

$$\dot{\boldsymbol{\eta}} = R(\psi)\boldsymbol{\nu} \tag{1a}$$

$$M\dot{\boldsymbol{\nu}} = -\big(C(\boldsymbol{\nu}) + D(\boldsymbol{\nu})\big)\boldsymbol{\nu} + B_\tau \boldsymbol{\tau}_c + \boldsymbol{\tau}_{\mathrm{w}} \tag{1b}$$

where

$$R(\psi) = \begin{bmatrix} \cos(\psi) & -\sin(\psi) & 0 \\ \sin(\psi) & \cos(\psi) & 0 \\ 0 & 0 & 1 \end{bmatrix} \tag{2}$$

is the rotation matrix and

$$M = \begin{bmatrix} m_{11} & 0 & 0 \\ 0 & m_{22} & m_{23} \\ 0 & m_{32} & m_{33} \end{bmatrix} = \begin{bmatrix} m - X_{\dot{u}} & 0 & 0 \\ 0 & m - Y_{\dot{v}} & m x_g - Y_{\dot{r}} \\ 0 & m x_g - N_{\dot{v}} & I_{zz} - N_{\dot{r}} \end{bmatrix} \tag{3}$$

describes the mass matrix with vessel mass m, hydrodynamic derivatives in SNAME notation $X_{\dot{u}}, Y_{\dot{v}}, Y_{\dot{r}}, N_{\dot{v}}, N_{\dot{r}}$, distance x_g of the origin 0_b to the center of gravity on the x_b-axis, and moment of inertia I_{zz}. Coriolis and centripetal effects are included in the matrix

$$C(\boldsymbol{\nu}) = -C(\boldsymbol{\nu})^{\mathrm{T}} = \begin{bmatrix} 0 & 0 & c_{13} \\ 0 & 0 & c_{23} \\ -c_{13} & -c_{23} & 0 \end{bmatrix}, \tag{4}$$

where

$$c_{13} = -m_{22} v - \frac{m_{23} + m_{32}}{2} r, \quad c_{23} = m_{11} u.$$

The damping matrix

$$D(\boldsymbol{\nu}) = -\begin{bmatrix} X_u + X_{|u|u}|u| & 0 & 0 \\ 0 & Y_v + Y_{|v|v}|v| & Y_r \\ 0 & N_v & N_r + N_{|r|r}|r| \end{bmatrix} \tag{5}$$

combines linear damping terms X_u, Y_v, Y_r, N_v, N_r and nonlinear second order modulus model terms $X_{|u|u}$, $Y_{|v|v}$, $N_{|r|r}$. For an underactuated surface vessel it holds that the effect of the control input $\boldsymbol{\tau}_c = [\tau_u\ \tau_r]^{\mathrm{T}}$ is applied with the actuator configuration matrix

$$B_\tau = \begin{bmatrix} 1 & 0 \\ 0 & 0 \\ 0 & 1 \end{bmatrix}. \tag{6}$$

The vector $\boldsymbol{\tau}_{\mathrm{w}}$ describes wind-induced disturbances. For a compact notation, the state vector $\boldsymbol{x} = [\boldsymbol{\eta}^{\mathrm{T}}\ \boldsymbol{\nu}^{\mathrm{T}}]^{\mathrm{T}} \in \mathbb{R}^n$, where $n = 6$ is the number of states, and input vector $\boldsymbol{u} = \boldsymbol{\tau}_{\mathrm{c}} \in \mathbb{R}^m$, where $m = 2$ is the number of inputs, are defined such that (1) can be rewritten in nonlinear input-affine form

$$\dot{\boldsymbol{x}} = \boldsymbol{f}(\boldsymbol{x}) + B\boldsymbol{u} + \overline{\boldsymbol{\tau}}_{\mathrm{w}}, \qquad t > 0, \quad \boldsymbol{x}(0) = \boldsymbol{x}_0 \tag{7a}$$

where

$$\boldsymbol{f}(\boldsymbol{x}) = \begin{bmatrix} R(\psi)\boldsymbol{\nu} \\ -M^{-1}\big(C(\boldsymbol{\nu}) + D(\boldsymbol{\nu})\big)\boldsymbol{\nu} \end{bmatrix}, \tag{7b}$$

$$B = \begin{bmatrix} \mathbf{0}^{(3\times m)} \\ M^{-1} B_\tau \end{bmatrix}, \tag{7c}$$

$$\overline{\boldsymbol{\tau}}_{\mathrm{w}} = \begin{bmatrix} \mathbf{0}^{(3\times 1)} \\ M^{-1}\boldsymbol{\tau}_{\mathrm{w}} \end{bmatrix}. \tag{7d}$$

2.2 Differential flatness

In the following, the differential flatness of the vessel model is shown. Theoretical background concerning differential flatness is provided in, e.g., Fliess et al. (1995); Rothfuß (1997); Fliess et al. (1999). The flat parameterization of the underactuated vessel model shows several singularities, see Agrawal and Sira-Ramirez (2004). Therefore, a fully actuated model with $\boldsymbol{u} = \boldsymbol{\tau}_c' = [\tau_u\ \tau_v\ \tau_r]^{\mathrm{T}}$ and $B = [\mathbf{0}^{(m\times 3)}\ (M^{-1}B_\tau')^{\mathrm{T}}]^{\mathrm{T}}$ where $B_\tau' = I^{(3\times 3)} = \mathrm{diag}\{1,1,1\}$ is assumed. Furthermore, the disturbance term in (7a) is neglected so that $\overline{\boldsymbol{\tau}}_w = 0$. Choosing the flat output $\boldsymbol{z} =$

$\boldsymbol{\eta} = [x\ y\ \psi]^{\mathrm{T}}$, the states and inputs can be differentially parametrized in the form

$$\boldsymbol{x} = \boldsymbol{\theta}_{\boldsymbol{x}}\big(\boldsymbol{z}, \dot{\boldsymbol{z}}, \ldots, \boldsymbol{z}^{(\boldsymbol{\beta}-\mathbf{1})}\big) = \begin{bmatrix} z_1 \\ z_2 \\ z_3 \\ \sin(z_3)\dot{z}_2 + \cos(z_3)\dot{z}_1 \\ \cos(z_3)\dot{z}_2 - \sin(z_3)\dot{z}_1 \\ \dot{z}_3 \end{bmatrix} \tag{8a}$$

$$\boldsymbol{u} = \boldsymbol{\theta}_{\boldsymbol{u}}\big(\boldsymbol{z}, \dot{\boldsymbol{z}}, \ldots, \boldsymbol{z}^{(\boldsymbol{\beta})}\big) = \begin{bmatrix} \theta_{\tau_u} \\ \theta_{\tau_v} \\ \theta_{\tau_r} \end{bmatrix}, \tag{8b}$$

with $\boldsymbol{\beta} = (2\ 2\ 2)$. The terms θ_{τ_u}, θ_{τ_v}, and θ_{τ_r} are provided in Appendix A. It becomes apparent that no singularities arise in (8).

To recover the original underactuated vessel dynamics from the flat parameterization of the fully actuated vessel it is necessary to impose the constraint

$$\theta_{\tau_v} = 0, \tag{9}$$

which induces an ODE in the components of $\boldsymbol{z}$. In principle, this ODE can be interpreted as the internal dynamics, see, e.g., the analysis in Rothfuss et al. (1996). For the considered OCP (9) is included by means of two inequality constraints to be fulfilled in terms of the decision variables.

2.3 Model parameters

The vessel parameters are taken from Do and Pan (2006) for a model ship and are summarized in Tab. 1. Therein, L_S and W_S are the vessel length and width, respectively. The inputs are constrained according to

$$-5\,\mathrm{N} \leq \tau_u \leq 5\,\mathrm{N}, \tag{10a}$$
$$-0.2\,\mathrm{N\,m} \leq \tau_r \leq 0.2\,\mathrm{N\,m}. \tag{10b}$$

Table 1. Vessel parameters

Mass matrix		Damping matrix linear		Damping matrix nonlinear		Vessel	
M_{11}	25.80	X_u	−12.0	$X_{\lvert u\rvert u}$	−2.1	L_S	1.20 m
M_{22}	33.80	Y_v	−17.0	$Y_{\lvert v\rvert v}$	−4.5	W_S	0.35 m
M_{23}	6.20	Y_r	−0.2	$N_{\lvert r\rvert r}$	−0.1	m	17.00 kg
M_{32}	6.20	N_v	−0.5				
M_{33}	2.76	N_r	−0.5				

3. FLATNESS-BASED OPTIMAL CONTROL

The aim for the desired approach is to generate trajectories while also considering actuator constraints. In other words, a combined trajectory-generation and motion control of the vessel is required while also taking into account confined environments for mooring maneuvers. In the following, CSG functions are discussed which can represent arbitrary shapes. These can be included to an OCP formulation. Furthermore, a flatness-based solution method for the OCP using B-splines is discussed.

3.1 Obstacle modeling

For obstacles of arbitrary shapes, CSG functions are used, see Ricci (1973). These are based on geometric primitive functions $f^{\mathrm{pr}}(\boldsymbol{x})$ such as ellipsoids, lines, and triangles. In order to describe the surface S of a shape mathematically, a function of the form

$$f^S(\boldsymbol{x}) \leq 1 \tag{11}$$

can be formulated which combines several primitive shapes using the maximum operator, i.e.

$$f^S(\boldsymbol{x}) = \max\left\{f_1^{\mathrm{pr}}(\boldsymbol{x}), \ldots, f_l^{\mathrm{pr}}(\boldsymbol{x})\right\}, \tag{12}$$

where l is the number of primitive functions used to define the shape. Since the gradient of the maximum operator is not smooth the approximation

$$\max\{f_1^{\mathrm{pr}}(\boldsymbol{x}), \ldots, f_l^{\mathrm{pr}}(\boldsymbol{x})\} \approx \big[(f_1^{\mathrm{pr}}(\boldsymbol{x}))^p + \ldots + (f_l^{\mathrm{pr}}(\boldsymbol{x}))^p\big]^{\frac{1}{p}} \tag{13}$$

is used, where the approximation quality increases with increasing $p \in \mathbb{N}$. In the following scenarios, rectangles are used to reflect confined areas. A rectangle can be constructed from two shifted and rotated parabolas, so that

$$f_{\mathrm{rect}}^S(\boldsymbol{x}|\boldsymbol{r}) = \left[\left(\frac{\cos(\alpha)(x-\tilde{x}_0) + \sin(\alpha)(y-\tilde{y}_0)}{d_x}\right)^{2p} + \left(\frac{-\sin(\alpha)(x-\tilde{x}_0) + \cos(\alpha)(y-\tilde{y}_0)}{d_y}\right)^{2p}\right]^{\frac{1}{p}}, \tag{14}$$

where the elements of $\boldsymbol{r} = [\tilde{x}_0\ \tilde{y}_0\ d_x\ d_y\ \alpha\ p]^{\mathrm{T}}$ describe the center position, length, width, orientation, and approximation quality parameter in the reference frame.

3.2 Problem formulation

In the following, the OCP for the considered system is expressed with

$$\min_{\boldsymbol{u}}\ J(\boldsymbol{u}) = \varphi(t_{\mathrm{f}}, \boldsymbol{x}(t_{\mathrm{f}})) \tag{15a}$$

s.t.

$$\dot{\boldsymbol{x}} = \boldsymbol{f}(\boldsymbol{x}) + B\boldsymbol{u}, \quad t > 0, \quad \boldsymbol{x}(0) = \boldsymbol{x}_0 \tag{15b}$$
$$\boldsymbol{g}\big(t_{\mathrm{f}}, \boldsymbol{x}(t_{\mathrm{f}})\big) = \mathbf{0} \tag{15c}$$
$$\boldsymbol{h}(\boldsymbol{x}) \leq \mathbf{0} \tag{15d}$$
$$\boldsymbol{u}^- \leq \boldsymbol{u} \leq \boldsymbol{u}^+, \tag{15e}$$

where $J(\boldsymbol{u})$ represents the cost functional in Mayer form that is to be minimized, t_{f} is the final time, (15b) denotes the ODE constraint imposed by the system dynamics with initial condition $\boldsymbol{x}(0) = \boldsymbol{x}_0$. Furthermore, terminal path constraints are included with (15c), and state constraints imposed by obstacles are formulated with (15d). Herein, $\boldsymbol{h}(\boldsymbol{x})$ is obtained by rearranging (11) and including (14) which yields $h_i(\boldsymbol{x}) = 1 - f_{\mathrm{rect},i}^S(\boldsymbol{x}), i = 1, \ldots, q$, where q is the number of rectangular obstacles. Input constraints are expressed using (15e), where $\boldsymbol{u}^-$, and $\boldsymbol{u}^+$ denote the lower and upper input bounds, respectively.

3.3 Flatness-based solution using B-splines

The ODE constraint (15b) is implicitly fullfilled by the flat parameterization (8) of the system. Therefore, the differential flatness of the vessel system can be exploited when the OCP is formulated in flat coordinates thereby eliminating the ODE constraint. Since the problem is still an infinite-dimensional it is convenient to parameterize the

flat outputs using B-spline functions which are unions of curve segements. For this, consider the expansion

$$z_j(t) \approx \hat{z}_j(t, \boldsymbol{p}_j) = \sum_{i=0}^{N_j} B_{i,D_j}(t) p_{i,j}, \quad \begin{matrix} t \in [0, t_\mathrm{f}], \\ j = 1, \dots, m \end{matrix} \tag{16}$$

for the jth component of the flat output $\boldsymbol{z}$. Herein, $B_{i,D_j}(t)$ are basis functions of order D_j and the vector $\boldsymbol{p}_j = [p_{0,j} \ \dots \ p_{N_j,j}]^\mathrm{T}$ summarizes the individual N_j weights. In general, the ability to approximate complex function behavior is improved as N_j is increased. Using B-spline functions the basis functions can be calculated recursively using the Cox-DeBoor scheme, see Piegl and Tiller (2013), i.e.

$$B_{i,0}(t) = \begin{cases} 1, & \text{for } t \in [u_i, u_{i+1}) \\ 0, & \text{else} \end{cases}, \tag{17a}$$

$$\begin{aligned} B_{i,j}(t) = &\frac{t - u_i}{u_{i+j} - u_i} B_{i,j-1}(t) \\ &+ \frac{u_{i+j+1} - t}{u_{i+j+1} - u_{i+j}} B_{i+1,j-1}(t). \end{aligned} \tag{17b}$$

In the recursion formula it can be seen that the time horizon $t \in [0, t_\mathrm{f}]$ is separated using a so-called knot vector

$$\hat{\boldsymbol{u}}_j = [u_{0,j} \ \dots \ u_{M_j,j}]^\mathrm{T} \quad j = 1, \dots, m. \tag{18}$$

At the knot points, the curve segments are joined to form the B-spline function. As can be seen from the recursion, the ith basis function $B_{i,D_j}(t)$ that is weighted with $p_{i,j}$ for the jth flat output is nonzero on the interval $t \in [u_{i,j}, u_{D_j+1,j})$. Thus, choosing

$$\hat{\boldsymbol{u}}_j = [\underbrace{0 \ \dots \ 0}_{D_j} \ 0 \dots \ t_\mathrm{f} \ \underbrace{t_\mathrm{f} \ \dots \ t_\mathrm{f}}_{D_j}]^\mathrm{T}, \tag{19}$$

results in $B_{k,0}(0) = 0$ for $k < D_j$ and only $B_{D_j,0}(0) = 1$, so that

$$\hat{z}_j(0, \boldsymbol{p}_j) = p_{0,j}. \tag{20}$$

Similarly, this choice of the knot vector yields $\hat{z}_j(t_\mathrm{f}, \boldsymbol{p}_j) = p_{N_j,j}$. In this way, initial and final values (of the flat outputs) are parameterized using the control points $p_{0,j}$ and $p_{N_j,j}$, respectively. The parameter M_j in $\hat{\boldsymbol{u}}$ can be determined with $M_j = D_j + N_j + 1$. The flat parameterization requires derivatives of the flat outputs up to order $\boldsymbol{\beta}$. The kth order derivative of a B-spline function is given by

$$\hat{z}_j^{(k)}(t, \boldsymbol{p}_j) = \sum_{i=0}^{N_j} B_{i,D_j}^{(k)}(t) p_{i,j}, \quad \begin{matrix} t \in [0, t_\mathrm{f}], \\ j = 1, \dots, m, \end{matrix} \tag{21}$$

where

$$\begin{aligned} B_{i,l}^{(k)}(t) = &\frac{l}{u_{i+l} - u_i} B_{i,l-1}^{(k-1)}(t) \\ &- \frac{l}{u_{i+l+1} - u_{i+1}} B_{i+1,l-1}^{(k-1)}(t), \quad \begin{matrix} k = 1, \dots, D_j - 1 \\ l = 0, \dots, D_j \end{matrix} \end{aligned}. \tag{22}$$

This means that the derivative of a B-spline function is again a B-spline function but of lower degree. Each B-spline function is $D_j - 2$ times continuously differentiable. To avoid numerical difficulties, D_j should be chosen as small as possible, i.e. $D_j = \beta_j + 2$. For further properties of B-spline functions, see Piegl and Tiller (2013). Substituting (16), (21) together with (8) into the OCP formulation (15) yields an equivalent problem with the new (constant) decision variables

$$\overline{\boldsymbol{p}} = \begin{bmatrix} \boldsymbol{p}_1^\mathrm{T} & \dots & \boldsymbol{p}_m^\mathrm{T} \end{bmatrix}^\mathrm{T} \in \mathbb{R}^{n_p}, \tag{23}$$

where $n_p = \sum_{j=1}^{m} N_j$ is the number of decision variables. Feasibility w.r.t. obstacle and input constraints (15d) and (15e), respectively, is checked at collocation points, $t_k = kh$, $k = 0, \dots, N$, where $N+1$ is the number of collocation points and $t_0 = 0$, $t_N = t_\mathrm{f}$. Consequently, a NLP is obtained.

4. MODEL PREDICTIVE CONTROL

In the following, the flatness-based OCP approach is extended to a MPC to compensate for wind-induced disturbances. This is done by repeatedly solving OCPs at discrete points in time with a step time of $\Delta t = t_\mathrm{MPC} = \text{const}$. As a scenario, a combined driving and mooring maneuver is considered, each resulting in a different OCP formulation.

4.1 Driving phase

In the first phase, the distance to a desired terminal position $(x_\mathrm{f}, y_\mathrm{f})$ is minimized within the fixed MPC time horizon $t_\mathrm{f} = t_\mathrm{hor}$, i.e.,

$$J(\boldsymbol{u}) = \varphi(t_\mathrm{f}, \boldsymbol{x}(t_\mathrm{f})) = (x(t_\mathrm{f}) - x_\mathrm{f})^2 + (y(t_\mathrm{f}) - y_\mathrm{f})^2, \tag{24}$$

with

$$\boldsymbol{g}(t_\mathrm{f}, \boldsymbol{x}(t_\mathrm{f})) = \emptyset, \tag{25}$$

such that no terminal condition is imposed on the problem. In this way, the closest point w.r.t. the terminal position is the solution to the OCP. It can be assumed that while driving no confined areas are passed by the vessel so that it is sufficient to adduce the origin 0_b of the body-fixed frame, i.e. (x, y), in order to evaluate the obstacle functions (15d).

4.2 Mooring phase

If the vessel origin is within a defined radius R_s (switching point) of the desired terminal position after an arbitrary iteration, the cost functional is altered to minimize the transition time, i.e.

$$J(\boldsymbol{u}) = \varphi(t_\mathrm{f}, \boldsymbol{x}(t_\mathrm{f})) = t_\mathrm{f}. \tag{26}$$

This requires the formulation of a terminal condition

$$\boldsymbol{g}(t_\mathrm{f}, \boldsymbol{x}(t_\mathrm{f})) = \boldsymbol{x}(t_\mathrm{f}) - \boldsymbol{x}_\mathrm{f}, \tag{27}$$

where $\boldsymbol{x}_\mathrm{f}$ is the arbitrary but fixed final state. In this phase, the vessel geometry is approximated as a rectangle and feasibility w.r.t. obstacles is ensured using four edge points of the rectangle.

4.3 Wind-induced disturbances

The disturbances induced by wind $\boldsymbol{\tau}_\mathrm{w}$ or $\overline{\boldsymbol{\tau}}_\mathrm{w}$, respectively, are calculated according to Fossen (2011) using a normally distributed wind direction $\beta_w \sim \mathcal{N}(\mu_\beta, \sigma_\beta)$ and an absolute wind velocity $V_{w,\mathrm{abs}} \sim \mathcal{W}(k_V, \lambda_V)$, where k_V and λ_V are shape and scale parameters of the Weibull distribution. With this, the forces and torque applied to the vessel can be calculated with

$$\boldsymbol{\tau}_\mathrm{w} = \frac{1}{2} \rho \big(V_{w,\mathrm{rel}}\big)^2 \begin{bmatrix} C_X A_f \\ C_Y A_l \\ C_N A_l L_S \end{bmatrix}, \tag{28}$$

where ρ is the air density, $V_{w,\mathrm{rel}}$ is the relative wind velocity which, together with the coefficients C_X, C_Y, and C_N, depends on the absolute wind direction β_w and speed $V_{w,\mathrm{abs}}$. The parameters L_S, A_f and A_l are vessel length, projected frontal and lateral areas, respectively.

Table 2. Obstacle and wind parameters.

	Obstacles				Wind			
	$\boldsymbol{r}_1$	$\boldsymbol{r}_2$	$\boldsymbol{r}_3$	$\boldsymbol{r}_4$				
$\tilde{x}_0$	2	2	0.5	3	A_f	$0.35\,\mathrm{m}^2$	μ_β	0 rad
$\tilde{y}_0$	17.575	18.575	16.325	10	A_l	$1.2\,\mathrm{m}^2$	σ_β	0.06 rad
d_x	2	2	1	1.5	L_S	1.2 m	λ_V	0.194
d_y	0.5	0.5	6	1.5			k_V	2
α	0	0	0	$\frac{\pi}{4}$			ρ	$1.205\,\frac{\mathrm{kg}}{\mathrm{m}^3}$
p	12	12	12	12				

5. SIMULATION RESULTS

Simulation results are generated in `MATLAB` using `CasADi` with `IPOPT` as NLP solver, see Andersson et al. (2018) and Wächter (2002), respectively. The underactuated vessel dynamics using the flat parameterization of the fully actuated system is retained by taking into account (9) which for numerical purposes is approximated by

$$-\epsilon \leq \theta_{\tau_v} \leq \epsilon, \tag{29}$$

for $\epsilon \ll 1$. For the simulation, only the solutions of θ_{τ_u}, and θ_{τ_r} are applied to the underactuated model.

Remark 1. Setting $\epsilon = 0$ would result in $N+1$ equality constraints which reduces the number of free decision variables in the NLP potentially rendering it unsolvable. Choosing $\epsilon > 0$ avoids this issue.

Initial and terminal (desired) states are chosen to be

$$\boldsymbol{x}_0 = \left[3.5\ 2\ \frac{\pi}{2}\ 0\ 0\ 0\right]^{\mathrm{T}}, \tag{30a}$$

$$\boldsymbol{x}_{\mathrm{f}} = [2.4\ 18\ 0\ 0\ 0\ 0]^{\mathrm{T}}. \tag{30b}$$

Further, the switching point is chosen to be

$$R_{\mathrm{s}} = t_{\mathrm{hor}}\sqrt{u_{\max}^2 + v_{\max}^2}, \tag{31}$$

where $u_{\max} = 0.38\,\mathrm{m/s}, v_{\max} \approx 0\,\mathrm{m/s}$ describe the maximum surge and sway velocity of the vessel, respectively. The fixed time horizon is set to $t_{\mathrm{hor}} = 15\,\mathrm{s}$ in the driving phase. The MPC horizon is shifted each iteration for $t_{\mathrm{MPC}} = 1\,\mathrm{s}$. Additionally, four obstacles are considered where $h_i(\boldsymbol{x}), i = 1,2,3$ are relevant for the mooring maneuver and $h_4(\boldsymbol{x})$ affects the driving maneuver. Feasibility w.r.t. constraints is ensured at $N+1 = 200$ collocation points. Additional scenario parameters are summarized in Tab. 2. The top view of the path, orientation, initial and final position, as well as the switching point are shown in Fig. 2a. It can be seen that there is no collision with any obstacle. Figure 2b shows the inputs with constraints marked using dashed-red lines which are satisfied for all times. The remainder of states is shown in Fig. 2c together with the switching time $t_s = 31\,\mathrm{s}$. Sudden changes in the inputs can be explained by numerical issues and disturbances which could push the vessel into the obstacles resulting in feasibility issues for the NLP solver. This could be avoided using soft constraints as described in Scokaert and Rawlings (1999).

6. CONCLUSION

In this paper a flatness-based MPC for an underactuated nonlinear surface vessel model is introduced. The fully actuated system is shown to be differentially flat so that

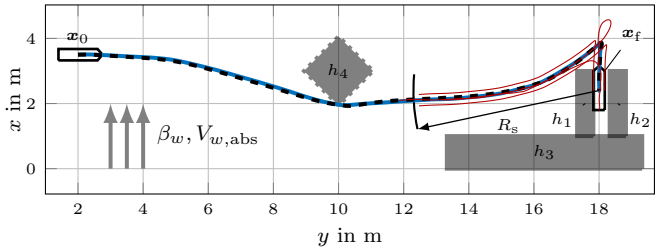

(a) Simulated path with wind direction β_w, absolute wind speed $V_{w,\mathrm{abs}}$, switching radius R_{d}, initial and final positions, and obstacles $h_i(\boldsymbol{x}), i = 1,\ldots,4$, as well as edge point paths in driving phase (red).

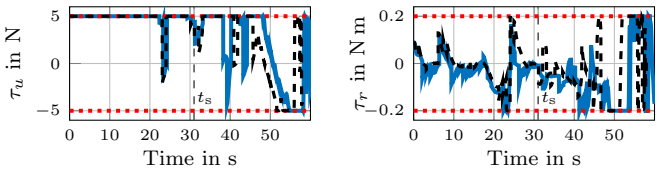

(b) Inputs surge force and yaw torque with constraints (dashed red). The input τ_v is not explicitly shown here because it is forced to zero.

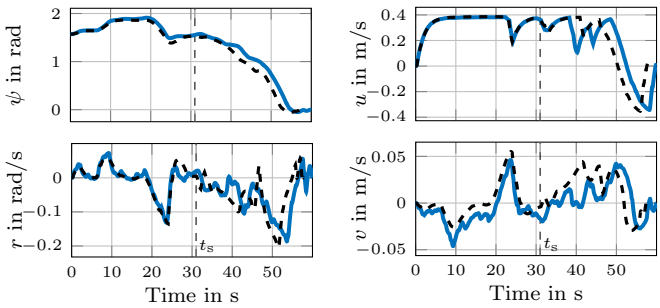

(c) Orientation and velocities of the vessel.

Fig. 2. Simulation results with optimal path (top), inputs (middle), and states (bottom) each with (blue) and without (black dotted) disturbances considering four rectangular obstacles.

the ODE constraint in the OCP can be removed. The flat outputs are parameterized using B-spline functions. A discretization in time of the OCP in flat coordinates allows the formulation of a NLP which can be solved numerically. Underactuated vessel dynamics are retained using inequality constraints imposed on the non-controllable input and obstacles are included to the OCP using CSG functions which can approximate arbitrary shapes. The concept is evaluated in a two-phase simulation scenario resulting in different OCP formulations. Future work focuses on real-time feasibility which can be achieved by approximating the highest-order derivative of each flat output and subsequent integration thus avoiding recursive computation of basis functions as shown in Oldenburg and Marquardt (2002). Further work also focuses on soft constraints and extending the concept to include collision avoidance regulations (COLREGS).

Appendix A. INPUT PARAMETRIZATION

The terms arising in (8b) read

$$\begin{aligned}\theta_{\tau_u} &= -X_{|u|u}\big(\sin(z_3)\dot{z}_2 + \cos(z_3)\dot{z}_1\big) \\ &\quad \cdot |\sin(z_3)\dot{z}_2 + \cos(z_3)\dot{z}_1| + m_{11}\sin(z_3)\ddot{z}_2 \\ &\quad - \big[(m_{22} - m_{11})\cos(z_3)\dot{z}_3 + X_u \sin(z_3)\big]\dot{z}_2 \\ &\quad - \big[(m_{11} - m_{22})\sin(z_3)\dot{z}_3 + X_u\cos(z_3)\big]\dot{z}_1 \\ &\quad - \frac{1}{2}(m_{23} + m_{32})\dot{z}_3^2 + m_{11}\cos(z_3)\ddot{z}_1,\end{aligned} \tag{A.1a}$$

$$\begin{aligned}\theta_{\tau_v} &= Y_{|v|v}\big(\sin(z_3)\dot{z}_1 - \cos(z_3)\dot{z}_2\big) \\ &\quad \cdot |\cos(z_3)\dot{z}_2 - \sin(z_3)\dot{z}_1| + M_{22}\cos(z_3)\ddot{z}_2 \\ &\quad + \big[(m_{11} - m_{22})\sin(z_3)\dot{z}_3 - Y_v\cos(z_3)\big]\dot{z}_2 \\ &\quad + \big[(m_{11} - m_{22})\cos(z_3)\dot{z}_3 + Y_v\sin(z_3)\big]\dot{z}_1 \\ &\quad + m_{23}\ddot{z}_3 - Y_r\dot{z}_3 - m_{22}\sin(z_3)\ddot{z}_1,\end{aligned} \tag{A.1b}$$

$$\begin{aligned}\theta_{\tau_r} &= m_{32}\cos(z_3)\ddot{z}_2 + m_{33}\ddot{z}_3 - N_{|r|r}\dot{z}_3|\dot{z}_3| - N_r\dot{z}_3 \\ &\quad + \big[(m_{22} - m_{11})\sin(z_3)\cos(z_3)\big]\dot{z}_2^2 \\ &\quad + \big[\big((m_{11} - m_{22})(\sin^2(z_3) - \cos^2(z_3))\big)\dot{z}_1 \\ &\quad + \frac{1}{2}(m_{23} - m_{32})\sin(z_3)\dot{z}_3 - N_v\cos(z_3)\big]\dot{z}_2 \\ &\quad + \big[(m_{11} - m_{22})\sin(z_3)\cos(z_3)\big]\dot{z}_1^2 \\ &\quad + \big[\frac{1}{2}(m_{23} - m_{32})\cos(z_3)\dot{z}_3 + N_v\sin(z_3)\big]\dot{z}_1 \\ &\quad - m_{32}\sin(z_3)\ddot{z}_1.\end{aligned} \tag{A.1c}$$

REFERENCES

Abel, D., Engelhardt, T., Konrad, T., and Schafer, B. (2016). Flatness-based control for a quadrotor camera helicopter using model predictive control trajectory generation. In *2016 24th Mediterranean Conference on Control and Automation*. IEEE.

Abel, D. and Joševski, M. (2015). Flatness-based Model Predictive Control for the Fuel Optimization of Hybrid Electric Vehicles. *IFAC-PapersOnLine*.

Agrawal, S.K. and Faiz, N. (1998). Optimization of a Class of Nonlinear Dynamic Systems: New Efficient Method without Lagrange Multipliers. *Optimization*.

Agrawal, S.K. and Sira-Ramirez, H. (2004). *Differentially Flat Systems*. Automation and Control Engineering. Taylor & Francis.

Andersson, J.A.E., Gillis, J., Horn, G., Rawlings, J.B., and Diehl, M. (2018). CasADi: a software framework for nonlinear optimization and optimal control. *Mathematical Programming Computation*.

Bårslett, S., Longva, M.N., and Nygård, T.i. (2018). *Auto-Docking of Vessel*. Ph.D. thesis.

Bitar, G., Breivik, M., and Lekkas, A.M. (2018). Energy-Optimized Path Planning for Autonomous Ferries. *IFAC-PapersOnLine*.

Bitar, G., Vestad, V.N., Lekkas, A.M., and Breivik, M. (2019). Warm-Started Optimized Trajectory Planning for ASVs.

Breivik, M. and Fossen, T.I. (2004). Path following for marine surface vessels. *Ocean '04 - MTS/IEEE Techno-Ocean '04: Bridges across the Oceans - Conference Proceedings*.

de Aquino Limaverde Filho, J.O. and Fortaleza, E.L.F. (2013). Motion Planning and Tracking for Marine Vessels. In *Volume 5: Ocean Engineering*. American Society of Mechanical Engineers.

Do, K.D. and Pan, J. (2006). Global robust adaptive path following of underactuated ships. *Automatica*.

Do, K.D. and Pan, J. (2009). *Control of Ships and Underwater Vehicles: Design for Underactuated and Nonlinear Marine Systems*.

Fliess, M., Levine, J., Martin, P., and Rouchon, P. (1995). Flatness and defect of non-linear systems: Introductory theory and examples. *International Journal of Control*.

Fliess, M., Lévine, J., Martin, P., and Rouchon, P. (1999). A lie-bäcklund approach to equivalence and flatness of nonlinear systems. *IEEE Transactions on Automatic Control*.

Fossen, T.I. (2011). *Handbook of Marine Craft Hydrodynamics and Motion Control*. John Wiley & Sons, Ltd, Chichester, UK.

Fossen, T.I., Breivik, M., and Roger Skjetne (2002). Line-of-Sight Path Following of Underactuated Marine Craft. *Science And Technology*.

Lekkas, A.M., Roald, A.L., and Breivik, M. (2016). Online Path Planning for Surface Vehicles Exposed to Unknown Ocean Currents Using Pseudospectral Optimal Control. *IFAC-PapersOnLine*.

Milam, M.B., Murray, R.M., and Mushambi, K. (2000). A New Computational Approach to Real-Time Trajectory Generation for Constrained Mechanical Systems. *Proceedings of the 39th IEEE Conference on Decision and Control*.

Oldenburg, J. and Marquardt, W. (2002). Flatness and higher order differential model representations in dynamic optimization. *Computers and Chemical Engineering*.

Paliotta, C., Lefeber, E., Pettersen, K.Y., Pinto, J., Costa, M., and Tasso de Figueiredo Borgesde de Sousa, J. (2018). Trajectory Tracking and Path Following for Underactuated Marine Vehicles. *IEEE Transactions on Control Systems Technology*.

Piegl, L. and Tiller, W. (2013). *The NURBS book*. Springer.

Ricci, A. (1973). A Constructive Geometry for Computer Graphics. *The Computer Journal*.

Rothfuss, R., Rudolph, J., and Zeitz, M. (1996). Flatness Based Control of a Nonlinear Chemical Reactor Model. *Automatica*.

Rothfuß, R. (1997). *Application of flatness-based analysis and control of nonlinear MIMO systems*. Ph.D. thesis, University of Stuttgart.

Scokaert, P.O. and Rawlings, J.B. (1999). Feasibility issues in linear model predictive control. *AIChE Journal*.

Streng, M. and Kuipers, B. (2020). Chapter 7 - economic, social, and environmental impacts of autonomous shipping strategies. In *Maritime Supply Chains*, 135 – 145. Elsevier.

Wächter, A. (2002). *An Interior Point Algorithm for Large-Scale Nonlinear Optimization with Applications in Process Engineering*. Ph.D. thesis, Carnegie Mellon University.